A Study on the Nonlinear Characteristics of Hydro-Pneumatic Suspension Systems for Mining Dump Trucks

Le Xuan Long
Faculty of Vehicle and Energy Engineering, Thai Nguyen University of Technology, Vietnam
lexuanlong@tnut.edu.vn

Le Van Quynh
Faculty of Vehicle and Energy Engineering, Thai Nguyen University of Technology, Vietnam
lequynh@tnut.edu.vn

Nguyen Van Tuan
Faculty of Vehicle and Energy Engineering, Thai Nguyen University of Technology, Vietnam
nltuan@tnut.edu.vn (corresponding author)

Nguyen Minh Chau
Faculty of Vehicle and Energy Engineering, Thai Nguyen University of Technology, Vietnam
minhchau-ice@tnut.edu.vn

Nguyen Khac Minh
Faculty of Vehicle and Energy Engineering, Thai Nguyen University of Technology, Vietnam
khacminhcdl@tnut.edu.vn

Received: 28 November 2024 | Revised: 24 December 2024 | Accepted: 1 January 2025

 DOI: https://doi.org/10.48084/etasr.9744

ABSTRACT

In the current study, nonlinear characteristics of Hydro-Pneumatic Suspension (HPS) systems for mining dump trucks are proposed and analyzed for the ride comfort of off-highway vehicles. To analyze these characteristics, a mathematical HPS model was used to determine the vertical elastic and damping forces. Then, a two-degrees-of-freedom (2-DOF) quarter-vehicle dynamic model of a mining dump truck was proposed to analyze the nonlinear characteristics of the HPS systems implemented in a MATLAB/Simulink environment under low-frequency excitations of road surfaces. An experiment was set up to measure the vibration accelerations at the upper and lower positions of the HPS systems to verify the proposed HPS mathematical model. The experimental and simulation results demonstrated that both the time- and frequency-domain accelerations were consistent with the laws of physics and exhibited errors within acceptable ranges, thereby demonstrating the reliability of the proposed mathematical model. The simulation results showed that the elastic force increased rapidly during the compression process and increased slowly during the rebound process, whereas the damping force increased very slowly during the compression process but increased rapidly during the rebound process owing to the effect of the backflow valve. The results of the force characteristic curve analysis of the HPS systems with different excitation frequencies also revealed that when the vibration excitation frequency increased, the elastic, damping, and vertical total forces of the front and rear HPS systems increased quite rapidly.

Keywords-mining dump truck; hydro-pneumatic suspension; elastic force; damping force

I. INTRODUCTION

HPS systems are often equipped on heavy trucks, especially off-highway trucks, owing to the good elasticity of the gas and the ability of HPS systems to reduce vibrations. Research on the characteristics of HPS systems is the basis for analyzing and evaluating their advantages and disadvantages, hence proposing solutions to enhance their performance. The nonlinear characteristics of the elastic and damping forces of the HPS systems have been analyzed through both

experimental and numerical methods, and the results have shown that the structural and physical parameters of the HPS systems significantly affect these characteristics [1-3]. The dynamic characteristics of the two types of interconnected HPS systems were investigated through a virtual experiment based on the AMEsim model, and the results disclosed that the structural parameters of the interconnected pipes and orifices of the HPS systems significantly affect HPS nonlinear characteristics [4]. Another similar study proposed a novel method for HPS modeling, which combines computational fluid dynamics simulation with approximate modeling, and can be used as a guide in the HPS design and control. The results showed that the physical parameters of the HPS systems greatly affect their nonlinear characteristics, and the model was experimentally verified with a prediction error lower than 5% [5]. To improve the stiffness and damping coefficient characteristics of the HPS systems, a Hydro-Pneumatic Inverter-Spring-Damper Suspension (HP-ISDS) system was proposed as a two-stage ISD suspension with a single structure, which used a type of dual chamber of HPS systems and was organically integrated using a fusion design method. The results demonstrated that HP-ISDSs significantly improved the vehicle ride comfort [6]. Anti-roll connected HPS systems were proposed to analyze the influence of amplitude and frequency excitations, flow coefficient, and initial pressure on the HPS systems motion state using nonlinear dynamics methods, and the results exhibited that the structural parameters of the HPS systems had a significant influence on their dynamic nonlinear characteristics [7]. The HPS characteristics, using a real gas multivariate index model, were verified under different survey conditions based on a full-vehicle experiment platform, and the results showed that a low excitation frequency greatly affects the nonlinear characteristics of the HPS systems [8]. A mathematical model for a Hydro-Pneumatic Interconnected Suspension (HPIS) system was proposed to analyze the influence of inertial fluids on its properties, and the results displayed that fluid inertia has a significant influence on the dynamic properties of HPISs [9]. The hydraulic actuator Semi-Active Suspension (SAS) system with two optimal controllers was proposed, and the results demonstrated that the effectiveness of the SASs significantly improved the vehicle ride comfort [10]. In a similar study, SAS system with magnetorheological struts were introduced, and the results indicated that the effectiveness of the SAS system significantly improved the vehicle ride comfort [11].

The ride effectiveness of the HPS systems mounted on off-highway trucks has been studied in terms of road surface friendliness [12, 13], under harsh conditions [14, 18], in comparison to rubber suspension systems [15], rubber and two types of leaf suspension systems [16], air suspension systems [17], and with two air suspension systems, regarding the road surface friendliness [19]. However, studies on the characteristics of the HPS systems of mining dump trucks are still quite limited, especially those of mining dump trucks under low-frequency and large-amplitude conditions of the off-highway road surfaces. In this study, a nonlinear mathematical model was established to determine the vertical nonlinear forces of the front and rear HPS systems of a mining dump truck. Subsequently, a DOF quarter-vehicle dynamic model is proposed to analyze the vertical forces of the HPS systems implemented in a MATLAB/Simulink environment under road surface excitations. To verify the proposed mathematical model, an experiment was conducted to measure the vibration accelerations at the upper and lower positions of the HPS systems. The characteristic curves of the elastic and damping forces and the total vertical force of the front and rear HPS systems were analyzed under low excitation frequency conditions of the road surfaces.

II. VEHICLE DYNAMIC MODEL

A structural schematic of the front and rear HPS systems is shown in Figure 1. Based on the structural diagram, the nonlinear dynamic model of the front and rear HPS systems is established through the stiffness and damping coefficients k_{hi} and c_{hi}, respectively, as portrayed in Figure 2. In Figure 1, the pressures of gas chamber A, main oil chamber B, and oil chamber C are denoted as p_{Ai}, p_{Bi}, and p_{Ci}, respectively. The inner diameter of the cylinder, the outer diameter of the rod, and the inner diameter of the HPS systems of the front axle are d_{a1}, d_{b1}, and $d_{c1,}$ respectively. The rod outer, inner, and inner diameters of HPS systems of the rear axle are d_{a2}, d_{b2}, and d_{c2}, respectively. The areas of the orifice and backflow valve are A_{1i} and A_{2i}, respectively. The vehicle axle and vehicle body displacements are z_{ai}, and z_{bi} (front axle, i=1 and rear axle, i=2).

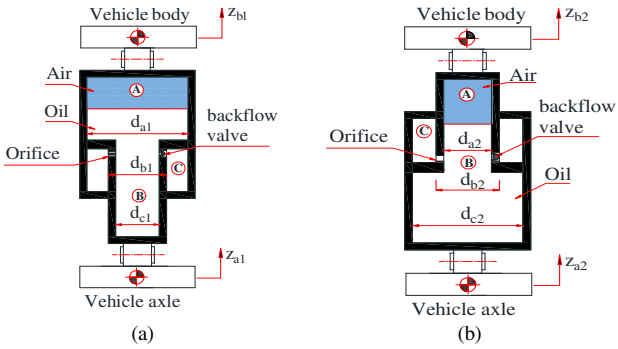

Fig. 1. Structural schematic of the (a) front and (b) rear HPS system.

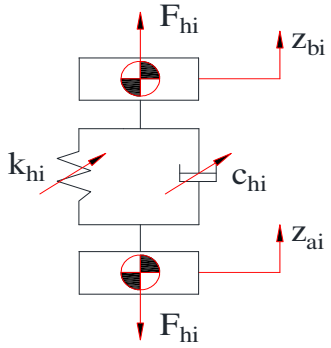

Fig. 2. Nonlinear dynamic model of HPS system.

From the nonlinear dynamic model depicted in Figure 2, it is derived that the total elastic and damping forces of the front and rear HPS systems can be determined using:

$$F_{hi} = F_{ki} + F_{ci} \quad (1)$$

where F_{hi}, F_{ki}, and F_{ci} are the vertical, elastic, and damping forces of the front and rear HPS systems, respectively.

A. The Elastic and Damping Force of Front HPS

The front HPS elastic force is created by the compressibility of gas in the air chamber, which can be determined using:

$$F_{k1} = (p_{A1} - p_{01})A_{b1} \quad (2)$$

where p_{0l} is the initial pressure of the air chamber in the front HPS.

The expansion of gas in the air chamber is considered an adiabatic process according to the laws of thermodynamics [20], and it can be determined utilizing:

$$p_{A1} = p_{01}\left(\frac{V_{01}}{V_{a1}}\right)^n, V_{a1} = V_{01} + A_{b1}(z_{b1} - z_{a1}) \quad (3)$$

where V_{01} is the initial volume of the air chamber of the front HPS, V_{a1} is the volume of the air chamber when the rod and cylinder are at any position, and n is the polytrophic rate.

By combining (2) and (3), the elastic force of the front HPS can be deduced by:

$$F_{k1} = p_{01}\left(\left(\frac{V_{01}}{V_{01}+A_{b1}(z_{b1}-z_{a1})}\right)^n - 1\right)A_{b1} \quad (4)$$

The front HPS damping force is created by the viscous resistance of the oil passing through the throttle hole between chambers B and C, and the frictional force between the piston and cylinder:

$$F_{c1} = (p_{a1} - p_{c1})(A_{a1} - A_{b1}) - F_{f1} \quad (5)$$

where F_{fl} is the friction force between the rod and cylinder of the front HPS.

The friction force between the rod and the cylinder of the HPS can be determined according to the wet lubrication theory [21]:

$$F_{f1} = \mu\frac{\pi d_{c1}L_1}{h_1}(\dot{z}_{b1} - \dot{z}_{a1}) \quad (6)$$

where μ is the dynamic viscosity coefficient of the oil, and L_l and h_l are the diameter of the rod and the thickness of the oil layer between the rod and the cylinder of the front HPS, respectively.

The pressure relationship between chambers B and C can be determined based on the oil flow through the throttle hole and check valve:

$$p_{C1} - p_{B1} = \frac{\rho(A_{a1}-A_{b1})^2(\dot{z}_{b1}-\dot{z}_{a1})^2 sign(\dot{z}_{b1}-\dot{z}_{a1})}{2C_d^2(A_{11}+0.5(1-sign(\dot{z}_{b1}-\dot{z}_{a1}))A_{21})^2} \quad (7)$$

where ρ is the density of the oil and C_d is the coefficient of discharge through the hole.

From (5), (6), and (7), the front HPS damping force can be obtained:

$$F_{c1} = -\frac{\rho(A_{a1}-A_{b1})^3(\dot{z}_{b1}-\dot{z}_{a1})^2 sign(\dot{z}_{b1}-\dot{z}_{a1})}{2C_d^2(A_{11}+0.5(1+sign(\dot{z}_{b1}-\dot{z}_{a1}))A_{21})^2}$$

$$-\mu\frac{\pi d_{c1}L_1}{h_1}(\dot{z}_{b1} - \dot{z}_{a1}) \quad (8)$$

B. The Elastic and Damping Force of Rear HPS

Similar to the front HPS, the elastic force of the rear HPS can be determined as:

$$F_{k2} = p_{02}\left(\left(\frac{V_{02}}{V_{02}+A_{b2}(z_{b2}-z_{a2})}\right)^n - 1\right)A_{b2} \quad (9)$$

The damping force of the rear HPS is:

$$F_{c2} = -\frac{\rho(A_{a1}-A_{b1})^3(\dot{z}_{b1}-\dot{z}_{a1})^2 sign(\dot{z}_{b1}-\dot{z}_{a1})}{2C_d^2(A_{11}+0.5(1+sign(\dot{z}_{b1}-\dot{z}_{a1}))A_{21})^2}$$

$$-\mu\frac{\pi d_{c2}L_2}{h_2}(\dot{z}_{b2} - \dot{z}_{a2}) \quad (10)$$

where L_2 and h_2 are the diameter of the rod and thickness of the oil layer between the rod and the cylinder of the rear HPS, respectively.

C. Quarter-vehicle Dynamic Model of a Mining Dump Truck

To analyze the nonlinear characteristics of the front and rear HPS systems, a 2-DOF quarter-vehicle dynamic model is established for analysis, with the vibration excitation source being sinusoidal road surface bumps with different frequencies, as displayed in Figure 3, where the vertical stiffness and damping coefficients of the tires are k_{ti} and c_{ti}, the front or rear axle and vehicle body displacements are z_{ai} and z_{bi}, respectively, and the road surface excitation is q.

The equation for the vehicle body motion is:

$$m_{bi}\ddot{z}_{bi} = F_{hi} \quad (11)$$

The equation of the vehicle axle motion is:

$$m_{ai}\ddot{z}_{ai} = F_{ti} - F_{hi} \quad (12)$$

where F_{ti} (i=1÷2) is the vertical force of the tire, which can be determined as:

$$F_{ti} = k_{ti}(z_{ai} - q) + c_{ti}(\dot{z}_{ai} - \dot{q}) \quad (13)$$

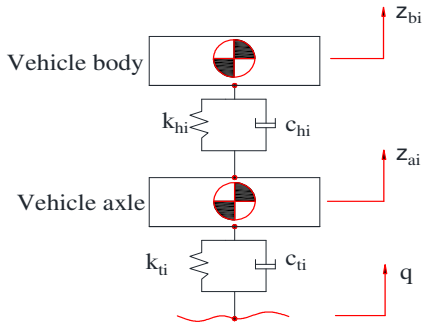

Fig. 3. A 2-DOF quarter-vehicle dynamic model.

D. Road Surface Roughness

The description of the road profile roughness using harmonic functions is usually a sinusoidal or cosine function. The advantage of a harmonic excitation source is that the input signal can be controlled; therefore, the evaluation of the output results will be more convenient.

If the vehicle moves at a constant speed v, the equation of the excitation function according to distance x can be written as:

$$q(x) = q_0 \sin\frac{2\pi}{T}t = q_0 \sin\frac{2\pi}{L}vt \quad (14)$$

where q_0, v, and L are the maximum height of the sine wave, the speed of movement, and the wavelength of the road surface, respectively.

III. EXPERIMENT

To verify the proposed HPS mathematical model, an experiment was conducted to measure the vibration accelerations at the upper and lower positions of the HPS systems when the vehicle moves on a single half-sinusoidal bump road surface, as depicted in Figure 4.

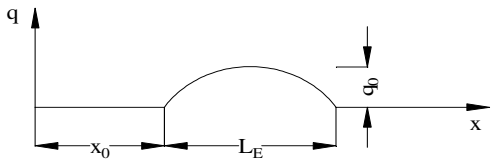

Fig. 4. Experimental single half-sinusoidal bump road surface.

The mathematical function of the single half-sinusoidal bump road surface is:

$$q = \begin{cases} 0: (x < x_0) \cup (x_0 + L_E < x) \\ q_0 sin\frac{2\pi}{2L_E}(x - x_0): (x_0 \le x \le x_0 + L_E) \end{cases} \quad (15)$$

where q_0 is the maximum height of the half-sine wave (q_0=0.065 m) and L_E is the length of the half-sine wave (L_E=0.64 m).

A vertical acceleration experiment was carried out, and the DEWEsoft signal processor was used to analyze the vibration accelerations in both the time and frequency domains with Kistler 8740A050B vibration sensors, which were transmitted to the DEWEsoft signal processor and connected to the computer for data processing, as shown in Figures 5 and 6. The comparison results between the experiment and the simulation of vertical time accelerations, and the Power Spectrum Density (PSD) of the accelerations above and below the positions of the HPS systems are illustrated in Figures 7–14. The results show that both the time- and frequency-domain accelerations are consistent with the laws of physics.

Fig. 5. DEWEsoft signal processor.

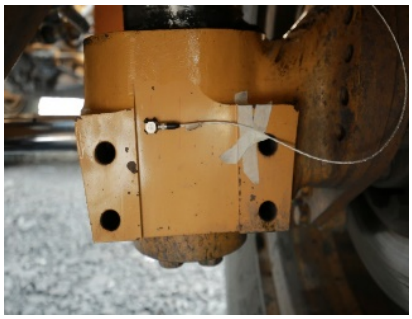

Fig. 6. Kistler 8740A050B vibration sensors.

From the results presented in Figures 7, 9, 11, and 13, the relative error of acceleration between the simulation and the experiment was calculated using:

$$e_a = \frac{\sqrt{\frac{\sum_{i=1}^{N}(a_{zsi} - a_{zei})^2}{N-1}}}{\frac{1}{N}\sum_{i=1}^{N}|a_{zsi}|} \quad (16)$$

where e_a is the relative error of the vertical acceleration, N is the number of the data points taken when the vehicle passes through a series of half-sine wave road surfaces, and a_{zsi} and a_{zei} are the vertical acceleration values according to the simulation and experiment at point i of the data points, respectively.

The relative error of the vertical time accelerations and the peak amplitude error of the PSD of the vertical accelerations' comparison between the simulation and experiment are listed in Table I. From Table I, it can be seen that the relative error of the vertical acceleration ranges from 9.67% to 12.86%. Based on the condition of the off-highway trucks and some assumptions to simplify the model, this error is acceptable. The analysis results demonstrate that the proposed mathematical model ensures reliability.

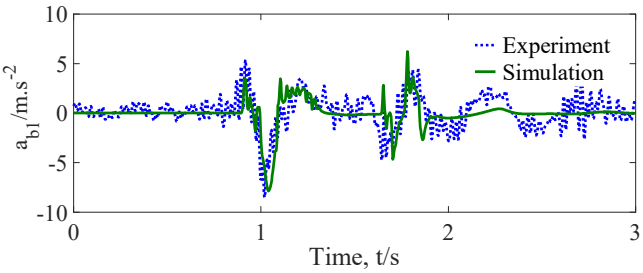

Fig. 7. Acceleration at the position above the front HPS.

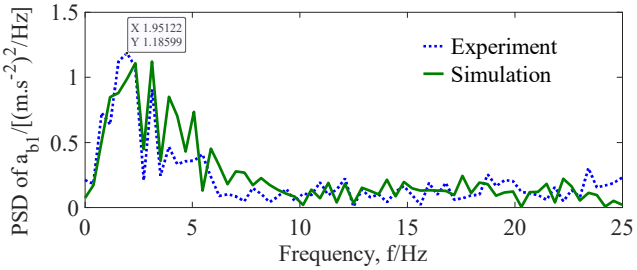

Fig. 8. PSD of a_{b1} at the position above the front HPS.

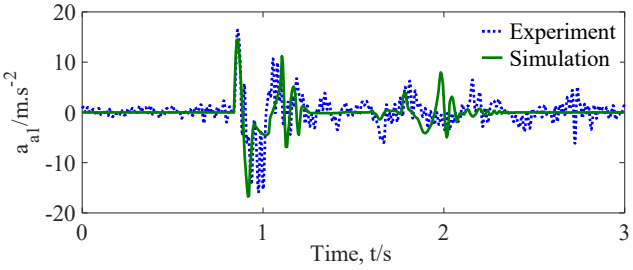

Fig. 9. Acceleration at the position below the front HPS.

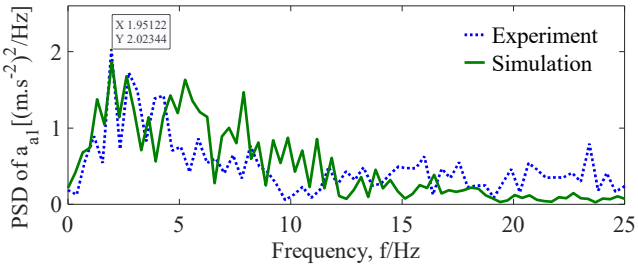

Fig. 10. PSD of a_{a1} at the position below the front HPS.

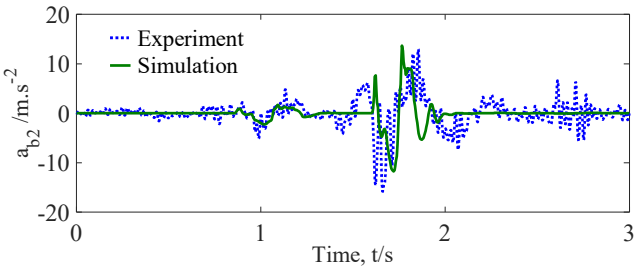

Fig. 11. Acceleration at the position above the rear HPS.

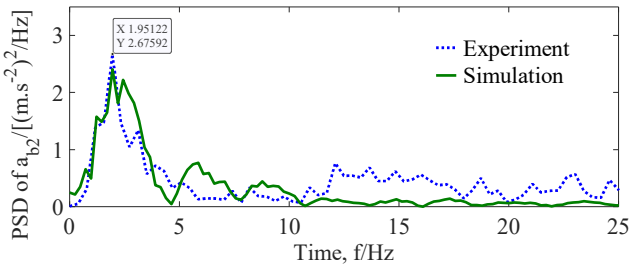

Fig. 12. PSD of a_{b2} at the position above the rear HPS.

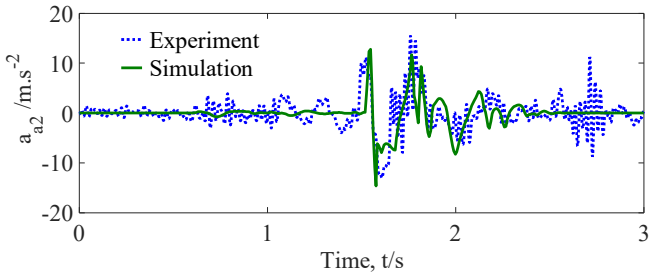

Fig. 13. Acceleration at the position below the rear HPS.

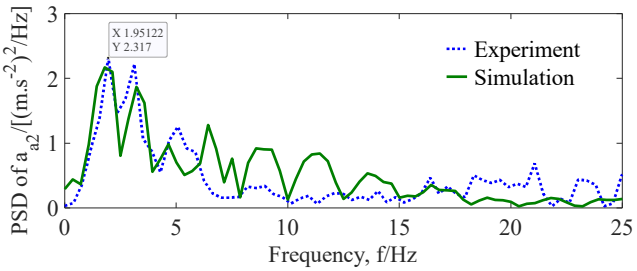

Fig. 14. PSD of a_{a2} at the position below the rear HPS.

TABLE I. ERROR PERCENTAGE RELATIVE TO VERTICAL TIME ACCELERATION AND PEAK AMPLITUDE VALUE ERROR OF PSD ACCELERATIONS BETWEEN SIMULATION AND EXPERIMENT

Positions	**b1**	**a1**	**b2**	**a2**
Vertical acceleration (%)	9.67	10.78	12.86	11.54
Peak amplitude of PSD of acceleration (%)	10.52	9.75	11.65	8.43

IV. RESULTS AND DISCUSSION

To analyze the nonlinear characteristics of the front and rear HPS systems, the nonlinear motion equations described above were solved in Matlab/Simulink environment, with the vehicle parameters of an off-highway truck caterpillar 773E being listed in Table II [22], referring to when the vehicle moves on a sinusoidal road surface bump with a bump height of q_0=0.05 m and with different low excitation frequencies and full load.

TABLE II. VEHICLE PARAMETERS OF AN OFF-HIGHWAY TRUCK

Parameter	**Value**	**Parameter**	**Value**
m_{a1}	1500 (kg)	p_{0airi}	14 (bar)
m_{a2}	3500 (kg)	V_{oili}	13 (dm^3)
m_{b1}	15800 (kg)	d_{a1}	20.3 (cm)
m_{b2}	27270 (kg)	d_{a2}	14 (cm)
k_{t1}	1.5e7 (N.m)	d_{b1}	17.8 (cm)
k_{t2}	3e7 (N.m)	d_{b2}	17.8 (cm)
d_{c1}	11.8 (cm)	d_{c2}	21.6 (cm)

The results of the vertical force of the HPS systems under sinusoidal vibration excitation at a frequency of f=4 Hz are shown in Figures 15-17.

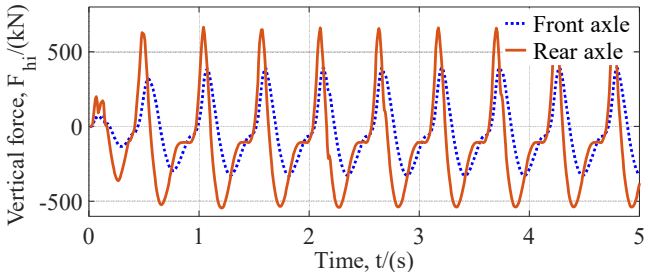

Fig. 15. Vertical force of HPS systems.

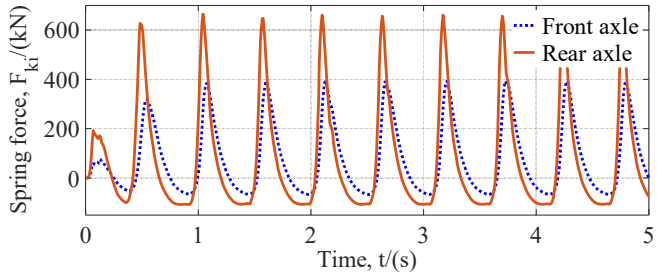

Fig. 16. Elastic force of HPS systems.

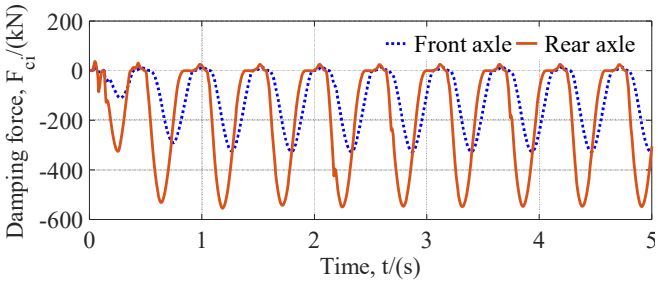

Fig. 17. Damping force of HPS systems.

Figures 15-17 demonstrate that the force peak amplitude values with the rear HPS are higher than those with the front HPS because the load distributed on the front HPS is smaller than that on the rear HPS, and the elastic, damping, and total vertical forces of the front HPS are significantly reduced compared to those of the rear HPS. The peak amplitude of the vertical force of the front HPS was reduced by 34.34% compared to that of the rear HPS. The results in Figure 16 show that the elastic forces of the front and rear HPS systems increase rapidly during the compression process and decrease slowly in the rebound process. The peak amplitude of the elastic force in the compression process is 6.18 times and 5.84 times larger than the peak amplitude in the rebound process. Figure 17 displays that the damping force increased rapidly in the rebound process and increased very slowly during the compression process, and the peak amplitude of the damping force in the rebound process was much larger than that in the compression process. This result is due to the influence of the backflow valve, which opens when the HPS systems are compressed and closes when HPS systems are in the rebound process. The characteristics of the elastic force, damping force, and total vertical force, depending on the excitation frequency, are further analyzed below.

A. Nonlinear Characteristics of Elastic Force

The elastic force characteristic curves according to the displacement and relative velocity between the rod and cylinder of the front and rear HPS systems are illustrated in Figures 18–21. According to Figures 18-21, the elastic force of the HPS systems increases rapidly and nonlinearly during the compression process and increases slowly and almost linearly in the rebound process. The graph of the relationship between the elastic force and the relative velocity between the rod and the cylinder shows that when the frequency of the excitation source increases, the elastic force peak amplitude in the compression process increases significantly, while the peak amplitude of the elastic force in the rebound process remains almost unchanged. The elastic force peak amplitude with the front HPS at low frequencies of f=2 Hz, f=3 Hz, and f=4 Hz increased by 33.96%, 61.32%, and 85.38%, respectively, compared to the low frequency at f=1 Hz, and it increased by 45.61%, 91.89%, and 121.28%, respectively, compared to the low frequency at f=1 Hz.

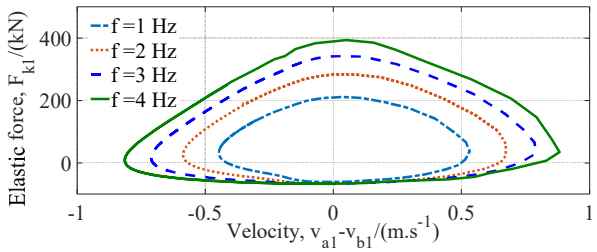

Fig. 18. Relationship between elastic force and velocity of the front HPS.

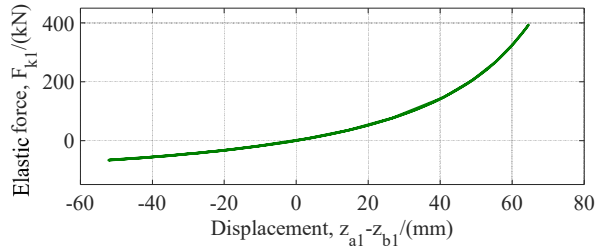

Fig. 19. Relationship between elastic force and displacement of the front HPS.

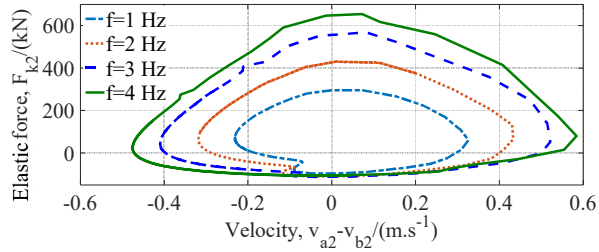

Fig. 20. Relationship between elastic force and velocity of the rear HPS.

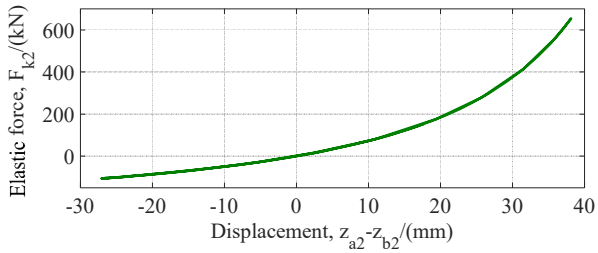

Fig. 21. Relationship between elastic force and displacement of the rear HPS.

B. Nonlinear Characteristics of Damping Force

The damping force characteristic curves of the front and rear HPS systems according to the velocity and relative displacement between the rod and cylinder under different low-frequency excitations of the road surfaces are depicted in

Figures 22-25. From the graph of the relation between the damping force and the relative displacement between the rod and the cylinder, it can be seen that the damping force increases rapidly during the rebound process but increases very slowly during the compression process owing to the effect of the backflow valve.

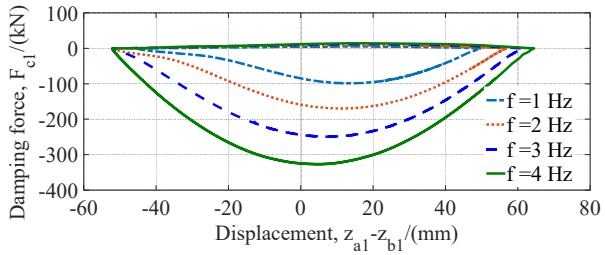

Fig. 22. Relation between damping force and displacement of the front HPS.

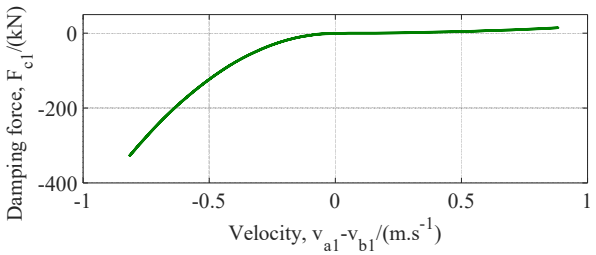

Fig. 23. Relationship between damping force and velocity of the front HPS.

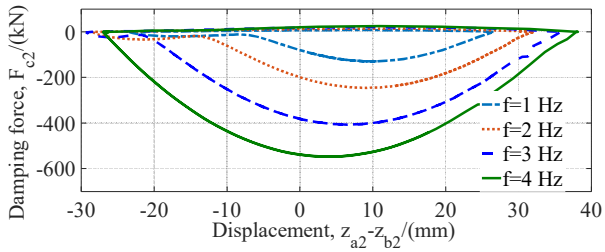

Fig. 24. Relation of damping force with displacement of the rear HPS.

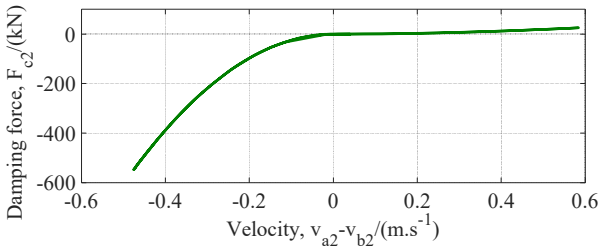

Fig. 25. Relationship between damping force and velocity of the rear HPS.

The results presented on the graph of the relationship between the damping force and the relative displacement between the rod and the cylinder (Figures 22-25) exhibit that when the value of the low-frequency excitation increases, the peak amplitude of the damping force in the compression process increases insignificantly and sharply during the rebound process. The peak amplitude of the damping force with the front HPS in the rebound process at the excitation frequencies of f=2 Hz, f=3 Hz, and f=4 Hz increased by 89.9%, 151.52% and 230.3%, respectively, compared to the low-frequency excitation at f=1 Hz, and increased by 90.7%, 215.5%, and 324.81%, respectively, compared to the low-frequency excitation at f= 1 Hz.

C. Nonlinear Characteristics of Total Vertical Force

The total vertical force is the total elastic and damping force of the HPS systems. The vertical force characteristic curves with the displacement and relative velocity between the rod and cylinder of the HPS systems of the front and rear axles are portrayed in Figures 26–29.

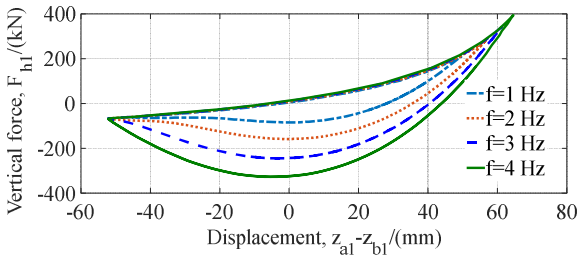

Fig. 26. Relationship between vertical force and displacement of the front HPS.

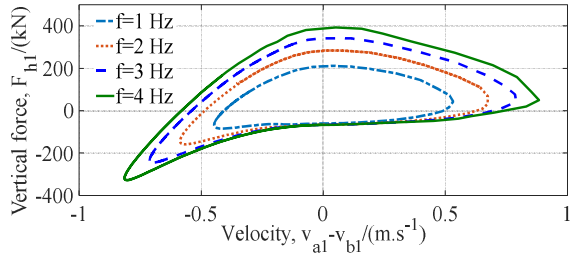

Fig. 27. Relationship between vertical force and velocity of the front HPS.

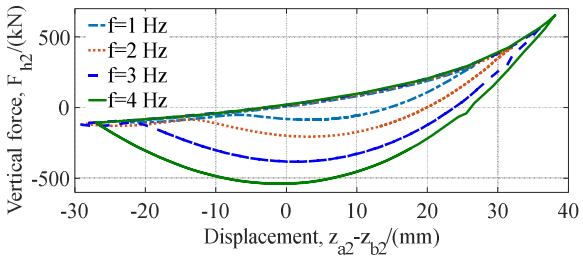

Fig. 28. Relationship between vertical force and displacement of the rear HPS.

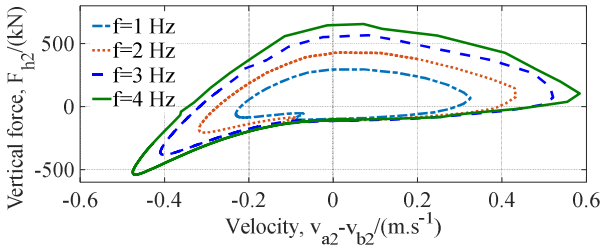

Fig. 29. Relationship between vertical force and velocity of the rear HPS.

The graphs demonstrating the relationship between the vertical force and the relative displacement between the rod and cylinder (Figures 26-29) show that the relative displacement between the rod and cylinder in the compression process increases, the vertical force increases quite quickly, and the vertical force decreases quickly when the displacement decreases. The relative displacement in the rebound process increased, the vertical force increased quickly, and the vertical force increased slowly when the relative displacement decreased. The graph between the vertical force and the relative velocity between the rod and cylinder, depicted in Figures 27 and 28, also exhibits that the relative velocity between the rod and cylinder in the compression process increases, the vertical force increases slowly, and the vertical force increases quite quickly when the velocity decreases. The relative velocity in the rebound process increased, the vertical force decreased quickly, and the vertical force increased quite quickly when the relative velocity decreased.

Figures 26–29 additionally show that as the low-frequency excitation value increases, the vertical forces of the front and rear HPS systems increase. The total vertical force of the front HPS at the low-frequency excitations at f=2 Hz, f=3 Hz, and f=4 Hz increased by 85.88%, 189.41%, and 285.88%, respectively, when compared to the low-frequency excitation at f=1 Hz, and the total vertical force of the rear HPS also increased by 139.53%, 344.19%, and 525.58%, respectively, when compared to the low-frequency excitation at f=1 Hz.

V. CONCLUSIONS

In this study, a nonlinear mathematical model of Hydro-Pneumatic Suspension (HPS) for a mining dump truck was developed to determine the elastic, damping, and total vertical forces. Subsequently, a two-degree-of-freedom (DOF) quarter-vehicle dynamic model was proposed to analyze the vertical forces of the HPS systems under low-frequency and large-amplitude off-highway road surfaces. An experiment was conducted to measure the vibration accelerations at the upper and lower positions of the HPS systems and to verify the HPS mathematical model. The following results were obtained. (i) The elastic force increased rapidly during the compression process and decreased slowly during the rebound process. The damping force increased rapidly in the rebound process and increased very slowly in the compression process, and the peak amplitude of the damping force in the rebound process was much larger than that in the compression process. (ii) The experimental and simulation results showed that both the time- and frequency-domain accelerations were consistent with the laws of physics and exhibited errors within acceptable ranges, thereby demonstrating the reliability of the proposed mathematical model. (iii) The elastic, damping, and total vertical forces of the front and rear HPS systems increased significantly when the frequency of the oscillating excitation source increased. The vertical force of the front HPS with low-frequency excitations at f=2, 3, and 4 Hz increased by 85.88%, 189.41%, and 285.88%, respectively. Similarly, the vertical force of the rear HPS increased by 139.53%, 344.19%, and 525.58%, respectively, for a low-frequency excitation of f=1 Hz.

ACKNOWLEDGMENT

The work described in this paper was supported by the Thai Nguyen University of Technology.

REFERENCES

[1] Y. Yin, S. Rakheja, J. Yang, and P.-E. Boileau, "Characterization of a hydro-pneumatic suspension strut with gas-oil emulsion," *Mechanical Systems and Signal Processing*, vol. 106, pp. 319–333, Jun. 2018, https://doi.org/10.1016/j.ymssp.2017.12.040.

[2] D. Lin, F. Yang, D. Gong, and S. Rakheja, "Design and experimental modeling of a compact hydro-pneumatic suspension strut," *Nonlinear Dynamics*, vol. 100, no. 4, pp. 3307–3320, Jun. 2020, https://doi.org/10.1007/s11071-020-05714-3.

[3] Y. Yin *et al.*, "Effects of Entrapped Gas within the Fluid on the Stiffness and Damping Characteristics of a Hydro-Pneumatic Suspension Strut," *SAE International Journal of Commercial Vehicles*, vol. 10, no. 1, pp. 204–209, Mar. 2017, https://doi.org/10.4271/2017-01-0411.

[4] D. Lin *et al.*, "Experimental Investigation of Two Types Interconnected Hydro-Pneumatic Struts," *IEEE Access*, vol. 7, pp. 100626–100637, 2019, https://doi.org/10.1109/ACCESS.2019.2931049.

[5] W. Wu, H. Tang, S. Zhang, L. Hu, and F. Zhang, "High-Precision Dynamics Characteristic Modeling Method Research considering the Influence Factors of Hydropneumatic Suspension," *Shock and Vibration*, vol. 2020, no. 1, 2020, Art. no. 8886631, https://doi.org/10.1155/2020/8886631.

[6] X.-L. Zhang, J. Liu, J. Nie, H. Wei, and L. Chen, "Simulation Analysis and Experiment Research on Hydro-Pneumatic ISD Suspension," *Shock and Vibration*, vol. 2021, no. 1, 2021, Art. no. 2095350, https://doi.org/10.1155/2021/2095350.

[7] J. Wang *et al.*, "Nonlinear dynamics and control of connected hydro-pneumatic suspension with fractional order," *International Journal of Non-Linear Mechanics*, vol. 157, Dec. 2023, Art. no. 104516, https://doi.org/10.1016/j.ijnonlinmec.2023.104516.

[8] Z. Li, Y. Wang, H. Du, and Z. Hu, "Modelling and analysis of full-vehicle hydro-pneumatic suspension system considering real-gas polytropic process," *Mechanical Systems and Signal Processing*, vol. 165, Feb. 2022, Art. no. 108406, https://doi.org/10.1016/j.ymssp.2021.108406.

[9] D. Lin, F. Yang, and R. Li, "Experimental modelling and analysis of compact hydro-pneumatic interconnected suspension strut considering pneumatic thermodynamics and hydraulic inertial properties," *Mechanical Systems and Signal Processing*, vol. 172, Jun. 2022, Art. no. 108988, https://doi.org/10.1016/j.ymssp.2022.108988.

[10] S. Babesse, "Design of Two Optimized Controllers of a Hydraulic Actuator Semi-Active Suspension: A Comparison Study," *Engineering, Technology & Applied Science Research*, vol. 9, no. 4, pp. 4561–4565, Aug. 2019, https://doi.org/10.48084/etasr.2836.

[11] R. N. Yerrawar and R. R. Arakerimath, "Parametric Analysis of Magnetorheological Strut for Semiactive Suspension System Using Taguchi Method," *Engineering, Technology & Applied Science Research*, vol. 8, no. 4, pp. 3218–3222, Aug. 2018, https://doi.org/10.48084/etasr.2139.

[12] L. X. Long, D. V. Ha, N. Van Tuan, V. T. Niem, and V. T. Hien, "A Simulation Investigation of Dynamic Wheel Load of a Heavy Truck with Hydro-Pneumatic Suspension System," in *Advances in Engineering Research and Application*, 2023, pp. 74–83, https://doi.org/10.1007/978-3-031-22200-9_8.

[13] L. X. Long, T. T. Hong, L. V. Quynh, and B. V. Cuongc, "Performance Analysis of the Hydropneumatic Suspension System of Heavy Truck," *International Journal of Mechanical Engineering and Technology*, vol. 9, no. 13, pp. 1128–1139, Jan. 2019.

[14] D. V. Ha, L. Van Quynh, and L. X. Long, "Performance Analysis of a Mining Dump Truck Ride Comfort with a Hydro-Pneumatic Suspension System under Different Operating Conditions," in *Advances in Engineering Research and Application*, 2023, pp. 790–797, https://doi.org/10.1007/978-3-031-22200-9_83.

[15] Long L. X., Hưng T. T., Tuấn N. V., and Hải L. X., "Ride performance analysis of a mining dump truck using hydro-pneumatic and rubber suspension systems under different road surface conditions," *Journal of Military Science and Technology*, no. FEE, pp. 183–189, Dec. 2023, https://doi.org/10.54939/1859-1043.j.mst.FEE.2023.183-189.

[16] L. X. Longa, L. V. Quynh, N. V. Liemb, B. V. Cuong, and H. A. Tand, "A Comparison of Ride Performance of Hydro-Pneumatic Suspension System with Those of Rubber and Leaf Suspension Systems," *IOP Conference Series: Materials Science and Engineering*, vol. 914, no. 1, Sep. 2020, Art. no. 012037, https://doi.org/10.1088/1757-899X/914/1/012037.

[17] L. X. Long, L. V. Quynh, N. V. Liem, B. V. Cuong, V. T. Hien, and H. A. Tan, "Ride Performance Evaluation of Air and Hydro-Pneumatic Springs of Suspension System," *International Journal of Advanced Research in Engineering and Technology*, vol. 12, no. 1, pp. 439–447, Jan. 2021.

[18] R. Jiao, V. Nguyen, and V. Le, "Ride comfort performance of hydro pneumatic isolation for soil compactors cab in low frequency region," *Journal of Vibroengineering*, vol. 22, no. 5, pp. 1174–1186, Aug. 2020, https://doi.org/10.21595/jve.2020.21345.

[19] V. Q. Le, "Comparing the performance of suspension system of semi-trailer truck with two air suspension systems," *Vibroengineering Procedia*, vol. 14, pp. 220–226, Oct. 2017, https://doi.org/10.21595/vp.2017.19224.

[20] K. Hutter and Y. Wang, *Fluid and Thermodynamics*, Springer, 2016.

[21] K. C. Ludema and L. Ajayi, *Friction, wear, lubrication: a textbook in tribology*, Second edition. Boca Raton: Taylor & Francis, CRC Press, 2019.

[22] "Medium Specalog for 773E Off-Highway Truck." AEHQ7983-02, 2019.